STATE DETECTION AND HYBRID SIMULATION OF BIOMEDICAL FLOWS

László Daróczy
Lab. of Fluid Dynamics & Technical Flows
University of Magdeburg "Otto von Guericke"
Universitaetsplatz 2, 39106 Magdeburg, Germany
Laszlo.Daroczy@ovgu.de

Abouelmagd Abdelsamie
Lab. of Fluid Dynamics & Technical Flows
Abouelmagd.Abdelsamie@ovgu.de

Gábor Janiga
Lab. of Fluid Dynamics & Technical Flows
Gabor.Janiga@ovgu.de

Domimique Thévenin
Lab. of Fluid Dynamics & Technical Flows
Dominique.Thevenin@ovgu.de

ABSTRACT

Hybrid simulations might be very interesting to save computational resources for a variety of applications involving different flow regimes. Combining proper models for laminar, transitional, or turbulent flows, described either by (U)RANS, LES or DNS depending on the needs, an accurate solution could then be obtained for complex configurations on existing computers. To do so, it is necessary to decide which kind of model should be used in which part of the numerical domain in space and time. As shown in this work, the spectral entropy S_d obtained from solving the eigenvalue problem for the temporal autocorrelation function, can be used in order to uniquely and automatically quantify the flow state and differentiate between laminar, transitional, or turbulent regime; as such, it delivers a direct measure of turbulence intensity. Using S_d, two hybrid simulations of biomedical flows have been carried out. The statistically-steady blood nozzle benchmark proposed by the FDA is simulated by URANS/LES, while the pulsating flow in a cerebral aneurysm is solved by LES/DNS. In both cases, savings in computational time and disk storage are observed, while keeping a very high accuracy.

1 INTRODUCTION

A criterion allowing to uniquely and automatically quantify the flow state and differentiate between laminar, transitional, or turbulent regime is essential to guide hybrid simulations, combining in the best possible way different simulation models (laminar flow equations; Reynolds-averaged Navier-Stokes approach – RANS; Unsteady RANS – URANS; Large-Eddy Simulations – LES; Direct Numerical Simulations – DNS;...). After identifying the flow state and quantifying turbulence intensity, a suitable approach can be implemented in an adaptive manner to combine proper models in space (different regions being computed using different numerical models), as shown in Davidson & Dahlström (2005)); and/or possibly in time, switching between different computational approaches as appropriate. Considering the rapid development of hybrid simulations (Sagaut *et al.*, 2013), identifying automatically the most appropriate model is becoming increasingly im-

portant. In order to be successful, hybrid simulations should ultimately rely on a user-independent and generally valid indicator of the flow state computed from the simulated flow field, as proposed in this work. Additionally, such an indicator could readily be used to guide in an automatic manner the resolution needed in space and time, so that, starting from a well-resolved – but time-consuming – computation, grid coarsening and/or larger timesteps could be used for part of the domain or the simulation, similar to what is done for embedded DNS (Cifuentes *et al.*, 2015). Finally, the same approach could also be used to automatically detect regions of interest (e.g., places where transition takes place) when analyzing large datasets. Such a procedure would be valuable for a variety of biomedical flows, in which laminar, transitional and turbulent regions are often found simultaneously, with considerable impact on clinical outcome (Byrne *et al.*, 2014).

2 SPECTRAL ENTROPY

The developed method was inspired by Snapshot Proper Orthogonal Decomposition (SPOD, see Sirovich (1987)), but for a completely different objective. The fundamental idea behind POD is to decompose each signal $\mathbf{u}(\mathbf{x}, t_k)$ into orthogonal deterministic functions ϕ (POD spatial modes) and time-dependent coefficients a_k (POD temporal coefficients):

$$\mathbf{u}(\mathbf{x}, t_k) = \sum_{l=1}^{\infty} a_k^l \, \phi^l(\mathbf{x}). \qquad (1)$$

Here, superscript l and subscript k refer to the mode number and index of corresponding snapshot (or timestep), respectively. The function ϕ denotes the eigenfunction of the Fredholm integral equation

$$\int_{\mathbf{X}} \mathbf{R}(\mathbf{x}, \mathbf{x}') \cdot \phi(\mathbf{x}') \, d\mathbf{x}' = \lambda \phi(\mathbf{x}). \qquad (2)$$

1

The kernel of this eigenvalue problem is the two-point spatial correlation function

$$\mathbf{R}(\mathbf{x}, \mathbf{x}') = \langle \mathbf{u}(\mathbf{x}, t_k) \otimes \mathbf{u}(\mathbf{x}', t_k) \rangle_t, \qquad (3)$$

where t_k and $\mathbf{x}$ are snapshot time and position vector, respectively. In POD, ϕ is chosen to maximize the value of $\langle |(\mathbf{u}, \phi)|^2 \rangle / \| \phi \|^2$, where $\langle \cdot \rangle_t$, $\langle \cdot \rangle$, $(\cdot, \cdot)$ and $\| \cdot \|$ are time average, spatial average, inner product and norm, respectively. Since the spatial modes ϕ^l are orthonormal to each other, the following equation can be used

$$\phi^l(\mathbf{x}) = \sum_{k=1}^{N_s} a_k^l \, \mathbf{u}(\mathbf{x}, t_k). \qquad (4)$$

In order to determine the coefficients a_k, Eq. (4) is substituted into Eq. (2), resulting in

$$\left(\frac{1}{N_s} \sum_{i=1}^{N_s} \mathbf{u}(\mathbf{x}, t_i) \otimes \mathbf{u}(\mathbf{x}, t_i), \sum_{k=1}^{N_s} a_k \mathbf{u}(\mathbf{x}, t_k) \right) = \lambda \sum_{k=1}^{N_s} a_k \mathbf{u}(\mathbf{x}, t_k),$$

where N_s is the total number of snapshots. Sirovich (1987) simplified this equation into

$$\sum_{k=1}^{N_s} \frac{1}{N_s} \left(\mathbf{u}(\mathbf{x}, t_i), \mathbf{u}(\mathbf{x}, t_k) \right) a_k = \lambda a_i \quad ; \quad i = 1, ..., N_s. \qquad (5)$$

Equation (5) can be rewritten in symbolic form as:

$$\mathbf{C}\mathbf{A} = \lambda \mathbf{A}, \qquad (6)$$

$$\mathbf{A} = (a_1, a_2, ..., a_{N_s})^T, \qquad (7)$$

$$C_{ij} = \frac{\left(\mathbf{u}(\mathbf{x}, t_i), \mathbf{u}(\mathbf{x}, t_j) \right)}{N_s}. \qquad (8)$$

Solving this eigenvalue problem, Eq. (6), leads to a total of N_s eigenvalues, written λ^l, and eigenvectors, denoted $\mathbf{A}^l$ ($l \in 1, 2, 3, ..., N_s$). When using SPOD for data analysis or data compression, it is not always necessary to keep all N_s modes. Then, M represents the number of modes retained in the analysis while N_s still represents the total number of snapshots, i.e., the whole data-set available for the analysis, obviously with $M \leq N_s$.

Equation (5) describes in general the eigenvalue problem based on the temporal autocorrelation function as kernel. The obtained eigenvalues represent the spectrum of the autocorrelation matrix ($\mathbf{C}$ in Eq. (6)). In order to characterize the intensity of the turbulence contained in the analyzed velocity field $\mathbf{u}$, the spectral entropy S_d is now computed. This quantity allows one to distinguish between different flow regimes, from "highly disordered" (here, meaning turbulence), to "partially ordered" (here, for transition), or "well ordered" (here, for laminar flow). For the computation of the spectral entropy, the relative energy P^l of mode
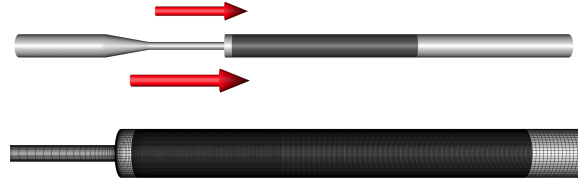
Figure 1. Hybrid configuration for the FDA benchmark nozzle. In the top figure the LES region is highlighted as dark gray. The bottom figure shows the corresponding mesh on the nozzle wall surface.

l is first computed based on the corresponding eigenvalue, after ordering them in decreasing order based on λ^l, as:

$$P^l = \frac{\lambda^l}{\sum_{j=1}^{M} \lambda^j}, \qquad (9)$$

where $M \leq N_s$ is the number of modes retained in the analysis. Then, the spectral entropy can be determined as:

$$S_d = -\sum_{l=1}^{M} P^l \ln P^l. \qquad (10)$$

According to Eq. (10), the maximum possible value of S_d is reached when all eigenvalues are equal to each other, i.e., $P^l = 1/M$, and consequently $S_d = \ln(M)$. Physically, this means that the energy is equally distributed over all the M modes. The minimum value of S_d corresponds to the case where the original signal contains only a single mode, the first one, meaning that the flow field is steady. Then, $S_d = 0$.

3 URANS/LES SIMULATION OF THE FDA BLOOD NOZZLE

The first application example investigates the performance of URANS/LES hybrid simulations for large-scale biomedical devices. Although CFD is now widely used for a broad range of industrial applications, most medical scientists still do not consider CFD as a mature tool for biomedical flow simulations. In order to check this point, the FDA (Food and Drug Administration) decided to propose several benchmark cases in order to check the validity and accuracy of CFD predictions for exemplary biomedical applications. The first one, considered here, is a blood nozzle (Stewart *et al.*, 2012). In spite of its relatively simple geometry (see top subfigure in Fig. 1), comparisons between CFD predictions and experimental results have revealed a poor agreement. A total of 28 CFD groups from all around the world participated in the blind study, considering five different Reynolds numbers ranging from Re = 500 to Re = 6500, computed using the throat diameter as typical length-scale. Laminar and RANS models were not able to deliver acceptable results. Subsequent studies have been able to achieve a much better agreement using LES (Delorme *et al.*, 2013; Janiga, 2014; Zmijanovic *et al.*, 2017), but obviously at a much higher computational cost. For the present study, the case with Re = 6500 is selected, since it is the most challenging one from the point of view of the flow state.

2

3.1 Computational setup

In order to deliver meaningful comparisons, the same simulation is executed twice, once relying completely on LES, and a second time starting with LES and switching to the hybrid URANS/LES approach based on the S_d indicator. For both simulations, the original setup is based on the recommendations of Janiga (2014). All simulations have been performed using the finite-volume solver ANSYS Fluent 17 with the pressure-based solver. The fluid is specified to be isothermal, incompressible and Newtonian. Concerning density and viscosity, 1056 kg/m^3 and 3.5 mPa.s are set, respectively, following the recommendations of the FDA challenge (Hariharan *et al.*, 2011). For the hybrid simulation, the Stress-Blended Eddy Simulation (SBES) approach is applied. In this approach, the user can provide the definition of the shielding function (f_{SBES}). This will decide which model is activated in a specific region by computing the turbulent viscosity:

$$\nu_t^{SBES} = f_{SBES}\nu_t^{URANS} + (1 - f_{SBES})\nu_t^{LES} \qquad (11)$$

A value of 1 specifies a URANS region (using here the $k - \omega - SST$ model), while a value of 0 denotes a LES region. For our application, the shielding function is defined based on the value of the spectral entropy, with $f_{SBES} = 0$ when $S_d \geq S_{d,crit.}$, where $S_{d,crit.}$ is the critical spectral entropy. Previous studies relying on Direct Numerical Simulations have shown that a spectral entropy around 0.46 represents the onset of transition. In order to stay on the safe side, a lower threshold of $S_{d,crit.} = 0.25$ is retained here, ensuring that LES is activated early enough for properly representing transition; this is impossible with a URANS approach.

The pure LES simulation corresponds simply to $f_{SBES} = 0$. In this way, one can use exactly the same setup for the LES and hybrid simulations; only the mesh and the shielding function have to be replaced.

At the nozzle inlet, a steady laminar parabolic velocity profile is prescribed, as the Reynolds number computed for the entry diameter is 2167, which is below the critical Reynolds number for pipes. However, a very low (0.5%) turbulence intensity was added, as proposed by Zmijanovic *et al.* (2017). In their study, they found that this improved the prediction of transition. Concerning the turbulence length scale, $0.07d_{pipe}$ is specified following users' guidelines. The outlet is defined as a pressure outlet. All walls are defined with standard no-slip boundary condition.

The Non-Iterative Time Advancement solver is chosen with the Fractional Step method. Instead of the second-order implicit temporal discretization, as done by Janiga (2014), the bounded second-order implicit scheme is retained, since this is required by SBES. To ensure an appropriately small CFL number, the timestep is chosen to be constant at 10^{-5} s.

3.2 LES and hybrid simulations

For the wall-resolved LES simulations, a fully structured hexahedral mesh is created with 18 million cells composed of hexahedral elements using two combined O-grid topologies. It is checked that the condition $y^+ \approx 1$ holds everywhere at the walls. The domain covers $x \in [-108; 180]$ mm, where $x = 0$ is the location of the sudden expansion in the blood nozzle. To initialize the flow-field, 30 000 timesteps are first executed. Afterwards, the computation is pursued until reaching 100 000 timesteps.
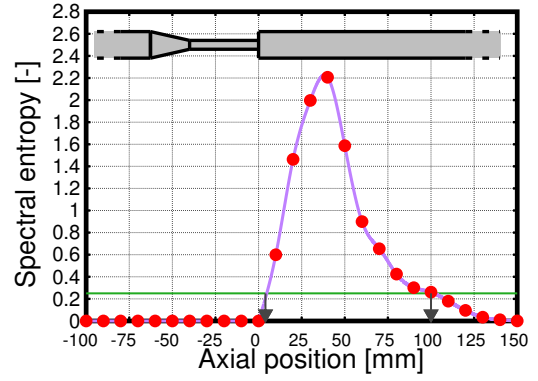
Figure 2. Spectral entropy along the axial position (based on the LES results within the time interval $[0.1, 0.13]$ s).

The obtained average velocity profiles indicate a very good agreement with the experimental data and with the previous numerical study, see Fig. 3.

In order to carry out the spectral entropy analysis, the hybrid simulation is started in exactly the same way, using the same mesh (18 million cells) with LES. Between timesteps 10 000 and 13 000 timesteps, every 10th timestep are exported for SPOD analysis. For the spectral computation, planar sections are defined perpendicular to the centerline at the discrete positions $x = [-100, -90, ..., 170, 180]$ mm. In each section, the instantaneous velocities are exported on a grid with resolution of 0.48 mm, resulting in the wider sections in 462, in the thinner sections in 52 data points. Finally, spectral entropy is computed as described in Section 2 using a Python script. The computation requires less than a minute. The result can be seen in Figure 2.

Based on S_d, the LES region is found to be in the region between 4 and 100 mm (Fig. 2); all other regions will switch to URANS mode. Of course, in URANS regions, a much coarser resolution is sufficient. Therefore, a second structured mesh is generated. It contains 9.5 million hexahedral cells, keeping the same resolution as previously within the LES region, but with a coarser mesh in the two URANS domains. After replacing the mesh, the simulation is restarted until reaching again 100 000 timesteps, activating the Vortex Method along the URANS-LES interface to generate velocity variations as input to LES based on the URANS turbulence intensity.

3.3 Comparisons

Experimental data have been obtained by independent PIV (Particle Image Velocimetry) measurements in three different laboratories (Hariharan *et al.*, 2011). As discussed in this publication, the different groups observed either laminar or transitional flows before reaching the throat for the considered Reynolds number. These different observations for the same configuration point out to one of the main challenges of the present case. While Re = 6500 corresponds clearly to turbulent conditions in the throat section, the corresponding Reynolds number computed with the diameter of the baseline pipe is Re = 2167, very close to the value classically associated to transition (Re$_c \approx 2200 - 2300$), so that laminar or transient conditions might be found due to spurious effects like slight vibrations in the surroundings or a pump inducing pulsations. Even very small disturbances

3
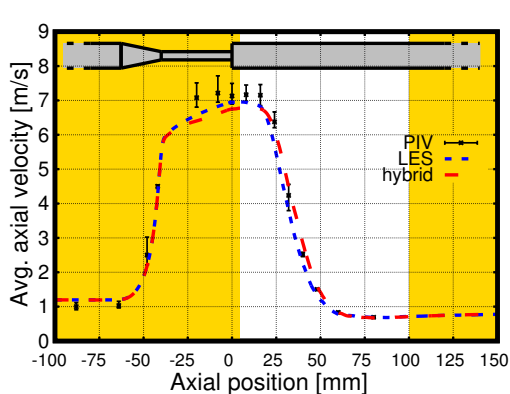
Figure 3. Averaged axial velocities along the centerline (the yellow region denotes URANS domains in the hybrid simulation).
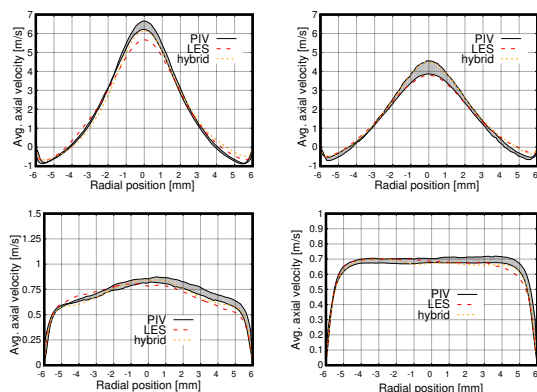
Figure 4. Averaged axial velocities along the cross-section at $x/D = 6$ (top left), $x/D = 8$ (top right), $x/D = 15$ (bottom left), $x/D = 20$ (bottom right), compared to PIV experimental data (grey corridor).

might be amplified and lead to different experimental observations.

All experimental results shown in what follows are the averaged values obtained by the three laboratories, as reported in Hariharan *et al.* (2011). The error bars (in Fig. 3) or the grey corridor (in Fig. 4) represent the deviation between the different measurements (min-max range). Figure 3 shows the computed time-averaged axial velocity along the centerline obtained by LES and hybrid simulation. The agreement of the pure LES simulation with the measurements is very good. Even more important, the agreement of the hybrid simulation with PIV in the central pipe is only slightly worse than with pure LES; it is at least as good in all other flow regions; and this good agreement is obtained at a reduced computational cost.

The available radial velocity profiles measured by PIV are compared with LES and hybrid simulation in Fig. 4. The agreement is very good in all cases. Due to the impact of URANS in the hybrid simulation, the obtained curves are slightly more symmetrical compared to the pure LES, and are therefore even closer to the PIV measurements. This is an indication that the averaging process is probably not completely finished yet in the pure LES simulation, while it is already attained in the hybrid simulation. This additional advantage is not reflected in the following runtime comparison.
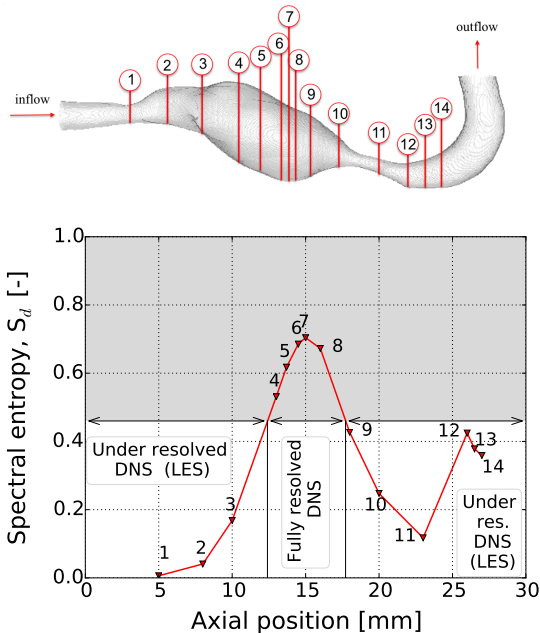
Figure 5. Spectral entropy values at different sections.

Both simulations have been carried out on the same system using 8 computer nodes, each equipped with a hexa-core Intel Xeon E5-1560v3 3.5 GHz processor, with a Gigabit Ethernet interconnection. Altogether, the run time was reduced by only 14%. Comparing only the last 70 000 timesteps, a speed- up of 19% is observed. Repeating the last 1000 timesteps on a single node with both approaches, the runtime was found to be proportional to the mesh size, leading now to a speed-up by 45% (almost a factor 2). Hence, the somewhat disappointing speed-up is due to the parallelization approach retained in ANSYS Fluent, possibly in combination with the slow (Gigabit Ethernet) processor interconnection. In order to solve such issues, access to the code sources is necessary. This explains why the second application example relies on our own Direct Numerical Simulation (DNS) tool, DINO.

4 LES/DNS SIMULATION OF A FUSIFORM ANEURYSM

The importance of transition to turbulence in cerebral aneurysms is a controversial topic (Byrne *et al.*, 2014), since it is still unclear if this might impact aneurysm rupture, often responsible for the death of the patient. Detecting the onset of transition in a complex geometry with a pulsatile flow requires accurate numerical models. This is why DNS is employed here as reference solution, using again spectral entropy S_d to guide hybrid LES/DNS simulations.

4.1 Computational setup

A patient-specific fusiform aneurysm (Fig. 5, top figure) provided by our partners at the Institute of Neuroradiology in Magdeburg was employed. The simulations are performed by DINO, our in-house finite-difference DNS tool, in which the complex geometry is handled by the immersed boundary technique. All details about the solver can be found in Abdelsamie *et al.* (2016). The fluid is considered incompressible and Newtonian.

Once again, two simulations are directly compared.

4

The reference one is obtained only by DNS. The hybrid simulation involves DNS in regions with high values of S_d, while the rest of the domain is still solved by the DNS solver, but with a noticeably coarser resolution, leading to an implicit LES simulation (Grinstein *et al.*, 2007). This is the most straightforward approach and is thus suitable for first tests. If those are successful, appropriate subgrid-scale models will be implemented in a next step. A pulsatile inflow condition mimicking appropriately the cardiac cycle in a brain artery is imposed.

For the fully-resolved DNS simulation, the spatial resolution in each direction is slightly below 60 μm, leading to 19 million grid points in the whole domain. The simulation is carried out for a complete cardiac cycle, storing the results each 800 iterations (i.e., 4 ms). Then, the spectral entropy S_d is computed by postprocessing the results for this cardiac cycle.

In our previous studies using the spectral entropy, a threshold $S_d \approx 0.46$ was used to delineate transition, with $S_d \ll 0.46$ corresponding to laminar flows. On the other side, $S_d > 1$ characterizes turbulent flows. The spectral entropy has been computed along fourteen two-dimensional cuts along the axial direction. These cuts are clustered near the region of interest, the fusiform aneurysm, as shown in Fig. 5 (top).

The obtained entropy values are depicted in Fig. 5 (bottom). In this figure, the shaded area corresponds to $S_d \geq 0.46$, where turbulence plays a noticeable role. This leads to a central region of the numerical domain where high-resolution DNS is always needed. On the other hand, the numerical domain up to an axial position of 12.40 mm (slightly before section 4) and after 17.72 mm (slightly before section 9) does not require such a resolution. There, the number of grid points can be noticeably reduced using a static but stretched mesh. At the end, the grid for hybrid simulations involves only 14 million grid points. The two regions with the coarser mesh are solved by implicit LES.

4.2 Comparisons

For the hybrid simulation, the finest grid size is still the same, while the largest grid size is 110 μm, as obtained by gradually stretching the mesh. It would be possible to reduce further the number of needed grid points by involving a subgrid-scale model.

The instantaneous maximum values of velocity magnitude in each cross-section up to plane #14 are shown at peak systole (time of 0.275 s) in Fig. 6. An excellent agreement between DNS and hybrid simulation is observed in the whole domain, with only minor deviations downstream of the aneurysm.

Figure 7 shows the temporal evolution of velocity magnitude at the section with the largest entropy value, being the most important one for practical purposes. Here also, an excellent agreement is observed.

The instantaneous flow field at peak systole is compared in Fig. 8 for all cut-planes. Confirming previous statements, an excellent agreement is observed both in the laminar region (sections #1 to 3) and in the region with high values of S_d (sections #4 to 9). Visible differences appear only in some later sections #12, 13 and 14, which might be avoided by improving near-wall resolution and/or activating an appropriate SGS model.

Each simulation has been carried out on 1024 processors of the high-performance computer SuperMUC at the Leibniz Supercomputing Center in Munich. Concerning
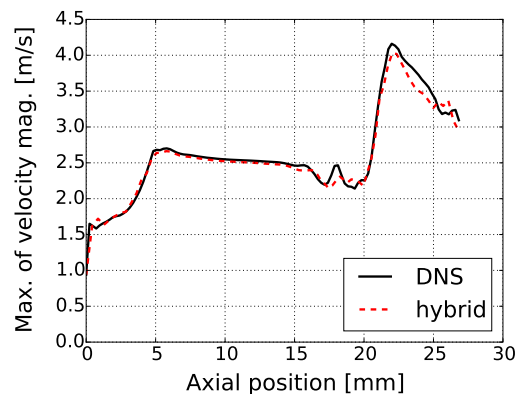
Figure 6. Maximum values of velocity magnitude along each cross section at peak systole.
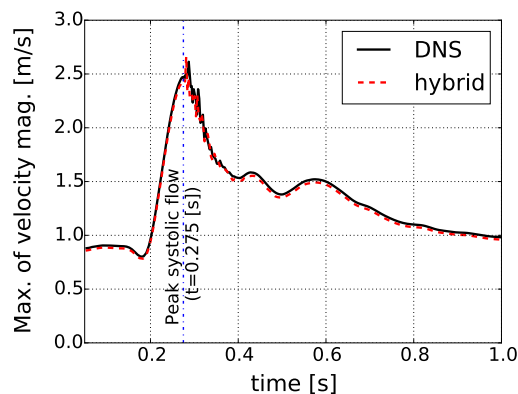
Figure 7. Temporal evolution of maximum value of velocity magnitude at section #7.

computational costs, the grid employed for the hybrid simulation is 26% smaller than for the high-resolution DNS, leading to a reduction of needed disk storage by the same amount. On the other hand, the obtained saving in computational time is only 15%. This is due to load-balancing issues in the hybrid simulation, and to a relatively large computational overhead induced in the current version of the code by solving the Poisson equation on a non-regular grid. After solving both issues, the savings in computing time should become similar to that in disk space in later studies.

5 CONCLUSIONS

In this article, spectral entropy S_d has been used to delineate between laminar, transitional and turbulent conditions for two important biomedical flows: the FDA blood nozzle benchmark, and the pulsatile flow in a fusiform aneurysm. Based on S_d obtained at high resolution, coarser meshes and simpler models have been activated in a hybrid simulation, combining URANS/LES for the blood nozzle, and LES/DNS for the aneurysm. In all cases, a close agreement is observed in the region of interest between the reference solution and the hybrid simulation results. A noticeable saving in storage is also observed, directly connected to the coarser mesh employed for the hybrid approach. On the other hand, the observed savings in terms of computing time are still limited: up to 19% for the blood nozzle, and 15% for the aneurysm case.

5
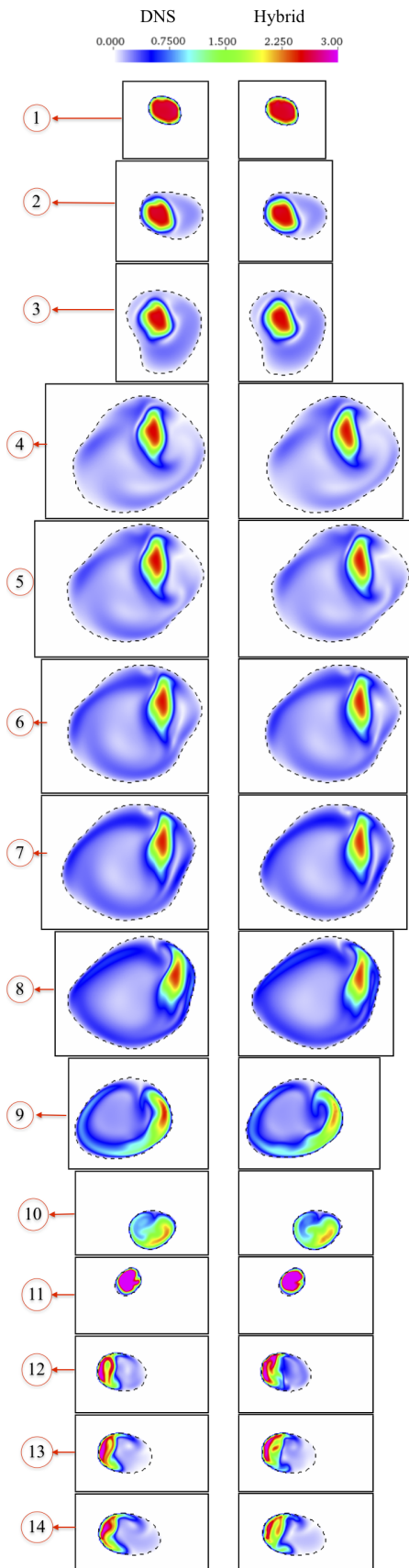
Figure 8.   2D cut-planes of velocity magnitude for all sections labeled in Fig. 5 at peak systole.

In both cases, parallelization and algorithmic issues on a non-regular grid have been identified as the main reason for this somewhat disappointing result. To get the best out of hybrid simulations, efficient parallel algorithms, fast communication networks and efficient load-balancing techniques must be implemented.

REFERENCES

Abdelsamie, A., Fru, G., Oster, T., Dietzsch, F., Janiga, G. & Thévenin, D. 2016 Towards direct numerical simulations of low-Mach number turbulent reacting and two-phase flows using immersed boundaries. *Comput. Fluids* **131**, 123–141.

Byrne, G., Mut, F. & Cebral, J. 2014 Quantifying the large-scale hemodynamics of intracranial aneurysms. *Am. J. Neuroradiol* **35**, 333–338.

Cifuentes, L., Dopazo, C., Martín, J., Domingo, P. & Vervisch, L. 2015 Local volumetric dilatation rate and scalar geometries in a premixed methane–air turbulent jet flame. *Proc. Combust. Inst.* **35**, 1295–1303.

Davidson, L. & Dahlström, S. 2005 Hybrid RANS-LES: An approach to make LES applicable at high Reynolds number. *Int. J. Comput. Fluid Dyn.* **19** (6), 415–427.

Delorme, Y.T., Anupindi, K. & Frankel, S.H. 2013 Large eddy simulation of FDA's idealized medical device. *Cardiovasc. Eng. Technol.* **4** (4), 392–407.

Grinstein, F.F., Margolin, L.G. & Rider, W.J. 2007 *Implicit Large Eddy Simulation*. Cambridge University Press.

Hariharan, P., Giarra, M., Reddy, V., Day, S. W., Manning, K. B., Deutsch, S., Stewart, S. F. C., Myers, M. R., Berman, M. R., Burgreen, G. W., Paterson, E. G. & Malinauskas, R. A. 2011 Multilaboratory particle image velocimetry analysis of the FDA benchmark nozzle model to support validation of computational fluid dynamics simulations. *J. Biomech. Eng.* **133**, 041002/1–14.

Janiga, G. 2014 Large eddy simulation of the FDA benchmark nozzle for a Reynolds number of 6500. *Comput. Biol. Med.* **47**, 113–119.

Sagaut, P., Deck, S. & Terracol, M. 2013 *Multiscale and multiresolution approaches in turbulence, LES, DES and hybrid RANS/LES methods*, 2nd edn. London: Imperial College Press.

Sirovich, L. 1987 Turbulence and the dynamics of coherent structures. Part 1: Coherent structures. *Q. Appl. Math.* **45** (3), 561–571.

Stewart, S.F.C., Paterson, E.G., Burgreen, G.W., Hariharan, P., Giarra, M., Reddy, V., Day, S.W., Manning, K.B., Deutsch, S., Berman, M. R., Myers, M.R. & Malinauskas, R.A. 2012 Assessment of CFD performance in simulations of an idealized medical device. *Cardiovasc. Eng. Technol.* **3** (2), 139–160.

Zmijanovic, V., Mendez, S., Moureau, V. & Nicoud, F. 2017 About the numerical robustness of biomedical benchmark cases. *Int. J. Numer. Method Biomed. Eng.* **33** (1), e02789.

6